catalysts

MDPI

Article

Facile Synthesis of Heterojunctioned ZnO/Bi_2S_3 Nanocomposites for Enhanced Photocatalytic Reduction of Aqueous Cr(VI) under Visible-Light Irradiation

Xiaoya Yuan *, Xue Wu, Zijuan Feng, Wen Jia, Xuxu Zheng and Chuanqiang Li

College of Materials Science and Engineering, Chongqing Jiaotong University, Chongqing 400074, China
* Correspondence: yuanxy@cqjtu.edu.cn; Tel./Fax: +86-23-62789154

Received: 18 June 2019; Accepted: 9 July 2019; Published: 21 July 2019

Abstract: Heterojunctioned ZnO/Bi_2S_3 nanocomposites were prepared via a facile solvothermal method. The obtained photocatalysts were characterized by X-ray powder diffraction (XRD), Scanning electron microscopy (SEM), High resolution transmission electron microscopy (HRTEM), X-ray photoelectron spectroscopy (XPS), UV-Vis diffuse reflectance spectroscopy (DRS), and Photoelectrochemical and Photoluminescence spectroscopy (PL), respectively. The results showed that ZnO/Bi_2S_3 composites exhibited the sandwiched-like structure, where ZnO nanoparticles were randomly embedded between Bi_2S_3 nanoflakes. The performance of photocatalytic Cr(VI) reduction under visible light indicated that ZnO/Bi_2S_3 composites exhibited high-efficiency photocatalytic activity in comparison with either Bi_2S_3 or ZnO. The 5%-ZnO/Bi_2S_3 photocatalyst removed 96% of Cr(VI) within 120 min at 20 mg/L initial concentration of Cr(VI). The enhanced performance of ZnO/Bi_2S_3 photocatalysts could be ascribed to the increased light harvesting and the effective separation and transfer of the photogenerated charge carriers across the heterojunction interface of the ZnO/Bi_2S_3 composite. This work could pave the way for the design of new hetero-structured materials and has great potential in environmental remediation.

Keywords: ZnO/Bi_2S_3; heterojunction; Cr(VI); photocatalytic reduction

1. Introduction

Hexavalent chromium (Cr(VI)) is a common oxidation state of chromium and is considered to be of acute toxicity, carcinogenicity and mutagen, which causes significant pollution to water and soil [1,2]. Currently, methods for disposing aqueous Cr(VI) include adsorption [3], reverse osmosis [4], ion exchange [5], etc. However, those means are commonly costly and nonrenewable. Lots of recent studies have shown that photocatalytic technology is regarded as a promising technique toward removing aqueous Cr(VI) because of the merits of cheap cost, high efficiency, simple fabrication, environment-friendly, and without discharge of undesirable chemicals [6–8]. As a consequence, the fabrication of efficient photocatalysts is inseparable to develop a high-performance photocatalytic process [9,10].

The well-known photocatalyst TiO_2 (E_g = 3.2 eV) is only sensitive to ultraviolet light and requires a mass of illumination time for the reduction of Cr(VI), which limits its practical application [11,12]. However, ultraviolet light is very little and only about 5% of the complete solar spectrum. Thence, it is desirable to manufacture innovative visible light-responsive photocatalysts to effectively enhance the removal of Cr(VI). Bi_2S_3 with a narrow band gap (E_g = 1.2~1.7 eV) has attracted great attention thanks to its strong visible-light absorption, no pollution and low cost [13,14]. Arpita Sarkar [15] et al. synthesized morphologically-tuned Bi_2S_3 NPs by a simple solvothermal method, which emerged

with 98% degradation toward methylene blue within 35 min under visible light irradiation. Enlai Hu [16] et al. synthesized Bi_2S_3 nanowires through a facile ethanol-assisted one-pot reaction, and it exhibited nearly 85.1% removal toward Cr(VI), which reduced within 60 min under visible light irradiation. Notwithstanding, the application of bare Bi_2S_3 is still limited as the recombination process of the photogenerated electron-hole pairs is fast. So many methods were developed to ameliorate the photocatalytic activity of Bi_2S_3 including morphology control [17], vacancy introduction [18], combination of other semiconductors [19], fabrication of heterojunction [20], incorporation of conductive materials (graphene) [21] or surface plasma resonance [22], etc. Among them, the fabrication of the heterojunction structure was a facile and effective method to improve the photocatalytic properties of the photocatalysts. The hole-electron pairs could be rapidly separated and transferred across the interface of the heterojunctioned photocatalyst. For example, some Bi_2S_3-based composites with heterojunctioned structure, such as BiOCl/Bi_2S_3 [23], Bi_2S_3/TiO_2 [24], Bi_2S_3/Bi_2WO_6 [25] and Bi_2S_3/BiOI [26], exhibited high catalytic activity towards different contaminants.

ZnO is one of photocatalyst commonly used in photolysis due to its good chemical stability, low cost, simple preparation, and non-toxicity [27,28]. The band alignment between ZnO and Bi_2S_3 is well matched from the point of theory, which indicates that they can be constructed into a heterojunctioned composite with expected enhancement of photocatalytic activity. The photogenerated electrons produced by photo-activated Bi_2S_3 can be transferred to the conduction band (CB) of ZnO, consequently promoting the separation of photoinduced carriers and prolonging the lifetime of the reactive oxygen species involved in the following photo-oxidation and photoreduction [29]. Therefore, it is reasonable to modify Bi_2S_3 with ZnO to increase the photocatalytic performance of the resulting hetero-junctioned composite.

In this study, ZnO/Bi_2S_3 photocatalyst with a heterojunctioned structure was prepared by a facile solvothermal method. The as-prepared composites were characterized by XRD, SEM, and HRTEM. The photocatalytic activity of ZnO/Bi_2S_3 heterojunctions was investigated by degrading Cr(VI) aqueous under visible-light ($\lambda > 420$ nm). On the basis of active species trapping experiments and the photocatalytic performance comparison with their counterparts, the mechanism of the enhanced Cr(VI) photoreduction by the prepared photocatalysts was further proposed.

2. Results and Discussion

2.1. Characterization of ZnO/Bi_2S_3 Photocatalysts Composites

XRD is utilized to analyze the purity and crystallographic structure of the as-prepared samples. Figure 1 displays the XRD patterns of pure ZnO, Bi_2S_3 and ZnO/Bi_2S_3 composites with different ZnO loadings. For pure ZnO, the typical peaks could be indexed to hexagonal wurtzite ZnO (JCPDS No. 36-1451) [30]. The diffraction peaks at $2\theta = 31.8°$, 34.3°, 36.4°, 47.3°, 56.5°, 62.9°, and 67.8° corresponded to (100), (002), (101), (102), (110), (103), and (112) planes of wurtzite ZnO crystals, respectively. For the pure Bi_2S_3 phase, the strong peaks appeared at 15.7°, 17.7°, 22.4°, 24.8°, 28.7°, 31.6°, 45.3°, 46.4°, and 52.6°, which could be indexed to (020), (120), (220), (130), (211), (221), (002), (431), and (351) planes of the standard Bi_2S_3 phase (JCPDS No. 17-0320) [31]. However, due to its low loading, the (110) peaks of ZnO in the composites could not be clearly detected in the XRD pattern. All diffraction peaks of the as-prepared composites matched exactly with those of pure ZnO and Bi_2S_3 phases and no other impurity peaks were detected, unambiguously indicating that ZnO/Bi_2S_3 composites were only composed of Bi_2S_3 and ZnO phases.

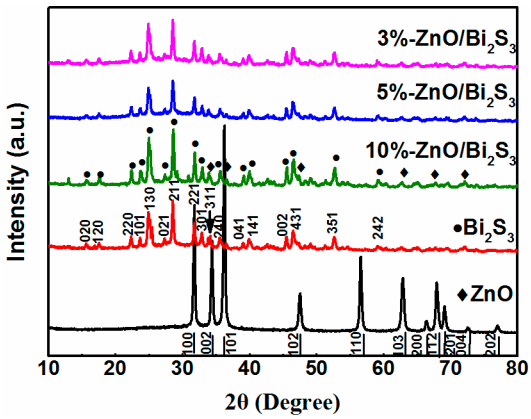

Figure 1. XRD patterns of ZnO, Bi_2S_3, and ZnO/Bi_2S_3 composites with different ZnO contents.

The morphologies of ZnO, Bi_2S_3 and 5%-ZnO/Bi_2S_3 samples are investigated by SEM. Pure ZnO exhibited a regular nanoparticles aggregate with an average particle size of ca. 60–80 nm (Figure 2a). Pure Bi_2S_3 presented sword-shaped thin nanoplates with lengths of ca. 9–15 um, thicknesses of ca. 1–1.8 um and some tiny irregular nanoparticles with an average particle size of ca. 30 nm (Figure 2b). Only Bi and S elements were detected from element mapping images (Figure S1) and their atomic ratio was 2:3, exactly equal to the theoretic formula of pure Bi_2S_3. 5%-ZnO/Bi_2S_3 sample exhibited the sandwiched-like structure, where some tiny nanoparticles were randomly embedded between the nanoflakes (Figure 2c). From Figure 2a,b, these nanoparticles would probably be either ZnO or Bi_2S_3. However, the elemental mapping showed (Figure S2) that Bi, S, Zn, and O could be observed throughout the prepared sample. This proved that sandwiched ZnO nanoparticles were randomly embedded, which demonstrated the existence of ZnO/Bi_2S_3 heterojunctions [32]. Besides, Compared with Figure 2b, the sheets of Bi_2S_3 became thinner and their lengths were reduced to 3~5 um. The sandwiched ZnO nanoparticles effectively prevented the re-stacking of lamellar Bi_2S_3 nanoplates. Additionally, from magnified Figure 2d, the ZnO nanoparticles were observed to be attached tightly to Bi_2S_3 nanoplates, thereby contributing to the fabrication of a heterojunction between ZnO and Bi_2S_3 within the composites.

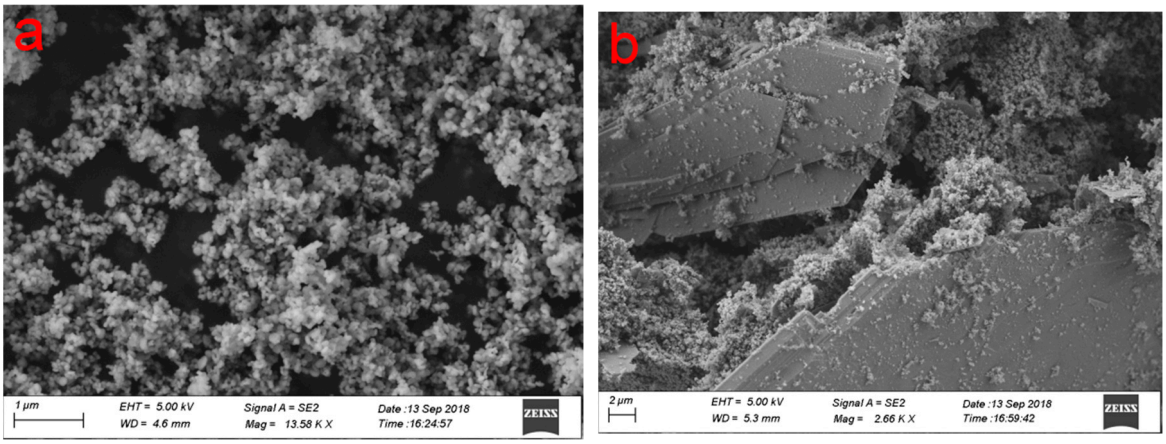

Figure 2. *Cont.*

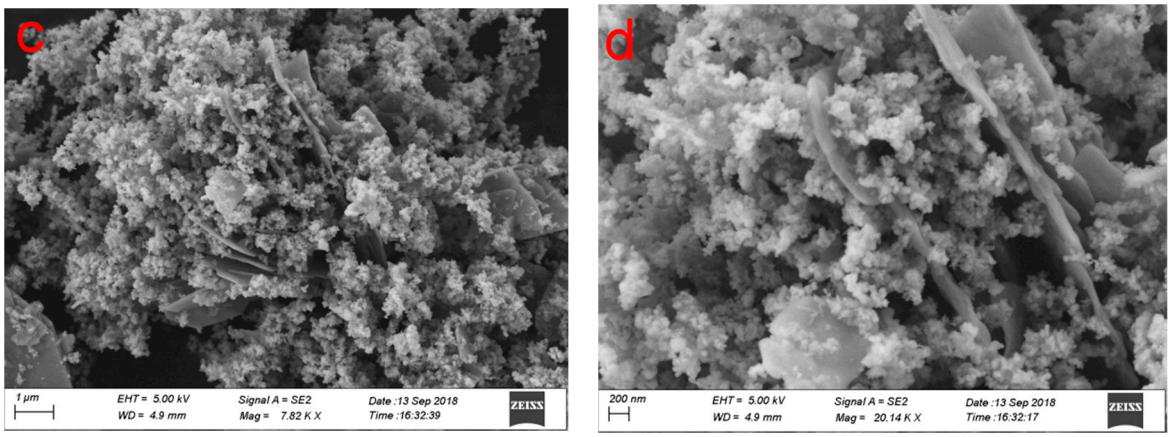

Figure 2. SEM images of as-prepared photocatalysts. (**a**) pure ZnO, (**b**) pure Bi_2S_3, and (**c**,**d**) 5%-ZnO/Bi_2S_3 composite.

More detailed structures of the 5%-ZnO/Bi_2S_3 sample are investigated by HRTEM, in which the interface of ZnO and Bi_2S_3 can be observed. Figure 3a manifests a large number of irregular nanosheets ranging in size from 200 to 500 nm. Furthermore, it could be seen that some tiny nanocrystals marked by a red circle in Figure 3a were conglutinated tightly to the nanosheets. Figure 3b exhibits a lattice image from the (100) planes with the interplaner spacing d (100) = 0.280 nm of ZnO [33] and that from the (130) planes with the interplaner spacing d (130) = 0.360 nm of Bi_2S_3 [34]. Moreover, intimate interface was clearly detected in Figure 3b and the heterojunction was somewhat preferably formed during the solvothermal fabrication of the 5%-ZnO/Bi_2S_3 composite [35,36]. The heterojunction structure within the prepared composite would favor the effective transfer of photo-induced carriers across the interface upon exposure to light and improve the photocatalytic performance of the resulting photocatalysts.

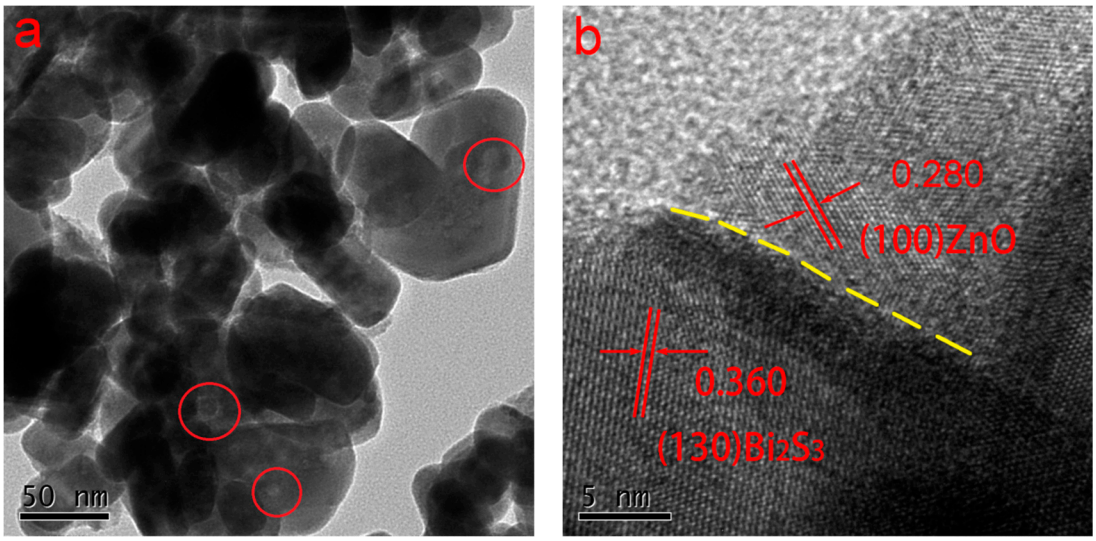

Figure 3. (**a**,**b**) HRTEM images of 5%-ZnO/Bi_2S_3 composite.

XPS is employed for the evaluation of chemical states of the elements in 5%-ZnO/Bi_2S_3 composites. The survey spectrum (Figure 4a) revealed that Bi, S, Zn, and O elements existed in this composite and Zn, Bi, and O elements were further analyzed from the spectra of Zn 2p, Bi 4f and O 1s. The main peaks at 1022.3 and 1044.9 eV were allocated to Zn $2p_{3/2}$ and Zn $2p_{1/2}$ (Figure 4b), respectively, verifying the existence of Zn^{2+} in the composite [37]. Figure 4c shows two strong peaks at 164.1 and 158.6 eV denoted as $Bi4f_{5/2}$ and $Bi4f_{7/2}$, respectively, revealing the existence of Bi^{3+} in the composite, which was consistent with other XPS results in Bi_2S_3 [26]. Also, as seen in Figure 4d, the O1s profile was asymmetric and

could be fitted into two symmetrical peaks at 530.0 and 531.8 eV, manifesting two different types of O species in the composite. The two peaks should be connected with the lattice oxygen (O–L) of ZnO and the chemisorption oxygen (O–H) caused by surface hydroxyl, respectively [38].

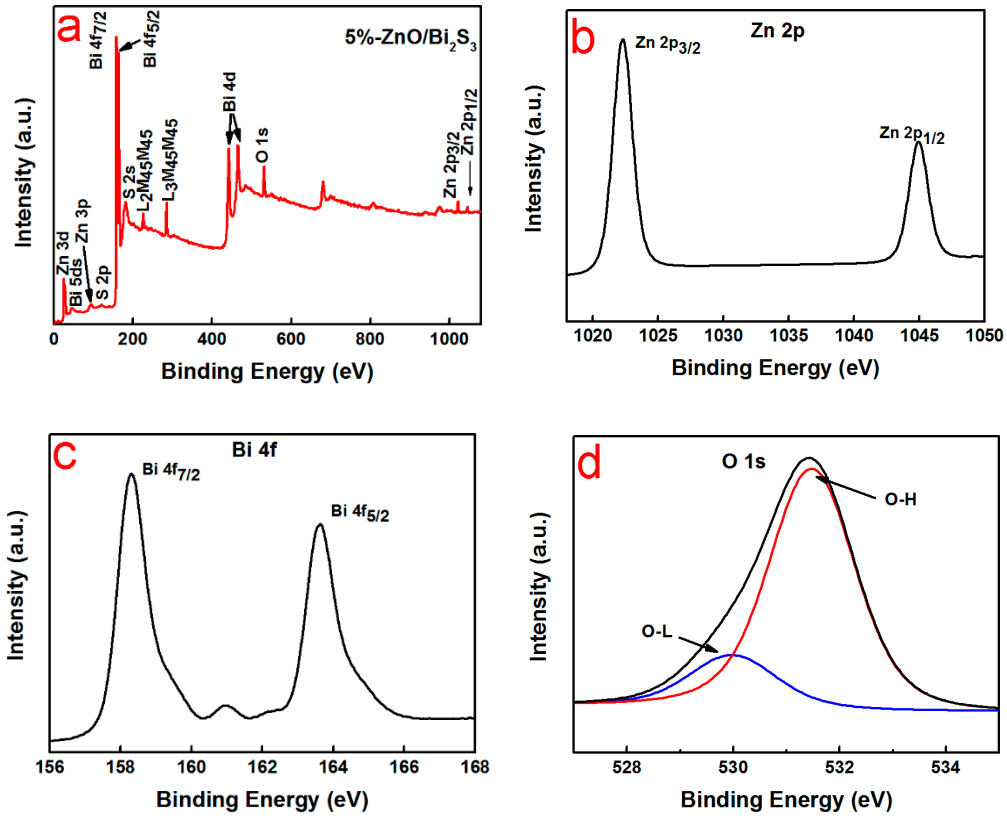

Figure 4. XPS spectra of 5%-ZnO/Bi_2S_3 composite: (**a**) survey scan, (**b**) Zn 2p, (**c**) Bi 4f, and (**d**) O 1s.

The DRS spectra of the as-synthesized 5%-ZnO/Bi_2S_3 nanocomposite as well as ZnO and Bi_2S_3 for comparison are shown in Figure 5a. It could be clearly observed that bare ZnO possessed strong UV light absorption, whereas it hardly absorbed light of the visible region. Bi_2S_3 and 5%-ZnO/Bi_2S_3 composites exhibited a similar light response profile and both showed strong absorption to the entire wavelength range. However, after the modification of ZnO, the absorbance of the composite to visible light was significantly enhanced, probably due to the synergistic absorption effect of the ZnO and Bi_2S_3 phase of the composite. The improved light response of ZnO/Bi_2S_3 unambiguously favored the photocatalytic performance of the prepared composite. Furthermore, using the Kubelka-Munk function (Equation (1)), one can count the band gap energy of bare ZnO, Bi_2S_3 and 5%-ZnO/Bi_2S_3 composite:

$$Khv = A(hv - Eg)^{\frac{n}{2}} \quad (1)$$

where E_g, v, A, h, and k are band gap energy, light frequency, a constant, planck constant, and the absorption coefficient. It had been reported that ZnO [39] and Bi_2S_3 [40] had n values of 1. The E_g value of ZnO, Bi_2S_3, and 5%-ZnO/Bi_2S_3 were estimated to be 3.20 eV, 1.60 eV, and 1.52 eV, respectively (Figure 4b). The bandgap of Bi_2S_3 was very close to the Sun's report [18]. In addition, the band gap energy was reported to be dependent on the size of crystal, but the conduction band (CB) potential is hardly affected by the size [15,16]. Obviously, the narrowed band gap of the ZnO/Bi_2S_3 nanocomposite was definitely helpful to the enhancement of the photocatalytic activity of the resulting composites.

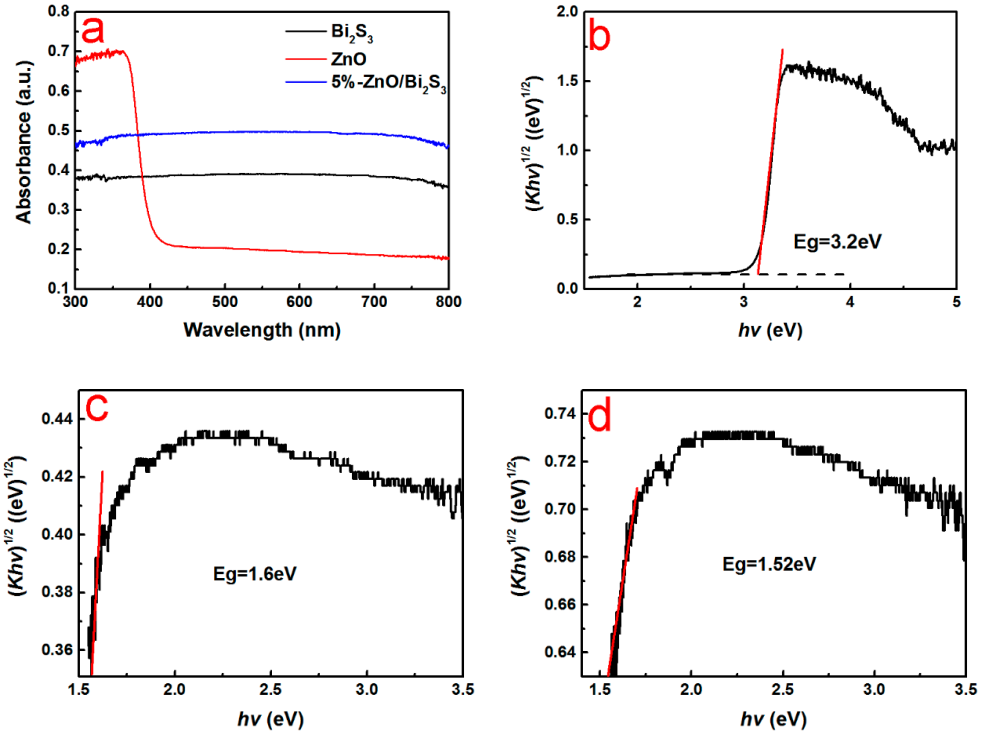

Figure 5. (**a**) UV-Vis spectra of ZnO, Bi_2S_3, 5%-ZnO/Bi_2S_3 composite; (**b**–**d**) plots of $(khv)^{1/2}$ versus hv of ZnO, Bi_2S_3, and 5%-ZnO/Bi_2S_3 composite.

Photocurrent measurement can also provide evidence for the separation rate of photo-generated carriers when the photocatalyst is excited by light. Figure 6 presents the transient photocurrent responses for pure ZnO, Bi_2S_3 and 5%-ZnO/Bi_2S_3 composite under visible-light irradiation. The current density of 5%-ZnO/Bi_2S_3 composite was dramatically increased, which was 10 times and 1.6 times that of bare ZnO and Bi_2S_3, indicating that photoelectron-hole pairs excited over 5%-ZnO/Bi_2S_3 composite were effectively separated and transferred across the heterojunction interface between ZnO and Bi_2S_3 within the composite.

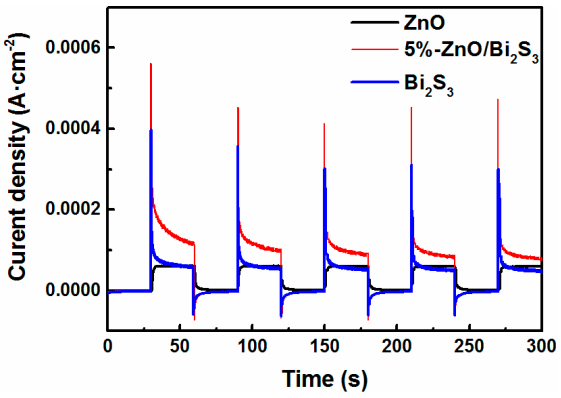

Figure 6. Transient photocurrent responses of ZnO, Bi_2S_3 and 5%-ZnO/Bi_2S_3 composite under visible light exposure.

The PL spectrum detects the separation efficiency of the electron-hole pairs for samples. It could be found that all the catalysts exhibited broad emission peaks around 450–500 nm (Figure 7). The smaller the PL intensity, the less recombination of the photogenerated charge carriers involved in the overall reaction [41]. Obviously, 5%-ZnO/Bi_2S_3 nanocomposite showed reduced PL intensity as compared to pure ZnO and Bi_2S_3, suggesting that the photo-generated charge carries for this composite were

effectively separated and their lifetime was prolonged, which was largely ascribed to the heterojunction structure within the ZnO/Bi_2S_3 composite.

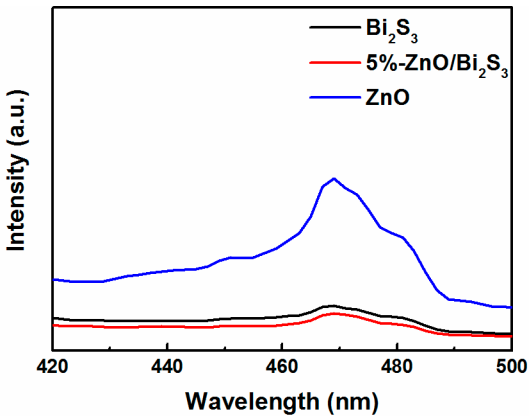

Figure 7. The PL spectra of ZnO, Bi_2S_3 and 5%-ZnO/Bi_2S_3 composite.

2.2. Photoreduction of Aqueous Cr(VI) Under Visible-Light Irradiation

Photocatalytic performances of the as-prepared photocatalysts were measured through the removal of Cr(VI) of 20 mg/L and catalyst dosage of 0.05 g under visible-light irradiation. After 1 h's dark adsorption, ZnO showed hardly adsorption ability towards aqueous Cr(VI). The adsorption removal ratio of 3%-ZnO/Bi_2S_3, 5%-ZnO/Bi_2S_3, 10%-ZnO/Bi_2S_3, and Bi_2S_3 for Cr(VI) were 43%, 33%, 45%, and 57%, respectively. Figure 8a reveals the variation of Cr(VI) concentrations with irradiation time catalyzed by the photocatalysts under visible light. The blank test (without photocatalyst) showed little photolysis under 2 h's visible light exposure, indicating that aqueous Cr(VI) was quite stable under visible-light irradiation. Upon irradiation, the solution containing Cr(VI) ions gradually lost its originally yellow color and the solution turned pale green. So the product of photocatalytic reduction of Cr(VI) would be Cr(III) ions [35]. The photoreduction rate toward Cr(VI) over pure ZnO and Bi_2S_3 was 10% and 77%, respectively. After modification of ZnO, the prepared composites had a higher photocatalytic performance than bare ZnO and pure Bi_2S_3. Compared with bare ZnO and Bi_2S_3, the catalytic activities of ZnO/Bi_2S_3 composites were significantly improved. The activity strongly depended on the ZnO content of the composites. When the content of Zno was increased, the photocatalytic activity of the composite was also increased, and 5% ZnO/Bi_2S_3 composite exhibited a maximum removal rate of 95%. However, further increasing the content of ZnO, the photocatalytic performance of the composite was reduced. To further compare the photocatalytic Cr(VI) reduction performance of the different samples, the pseudo-first-order reaction kinetic model was used to determine the photoreduction apparent reaction rate constants (k), where $-\ln(C/C_0)$ versus t were delineated (Figure 8b). The k values of different samples were in the following order: 5%-ZnO/Bi_2S_3 > 3%-ZnO/Bi_2S_3 > 10%-ZnO/ Bi_2S_3 > Bi_2S_3 > ZnO. The k value of 5%-ZnO/Bi_2S_3 was 30-fold that of virgin ZnO and 2.27-fold that of bare Bi_2S_3, further indicating that the photocatalytic Cr(VI) reduction activity of ZnO/Bi_2S_3 was highly dependent on the loading of ZnO, and the photocatalytic performance of Bi_2S_3 toward Cr(VI) removal was greatly promoted by incorporating the ZnO component. Therefore, the 5%-ZnO/Bi_2S_3 composite was employed to further investigate its photocatalytic activity in the following study.

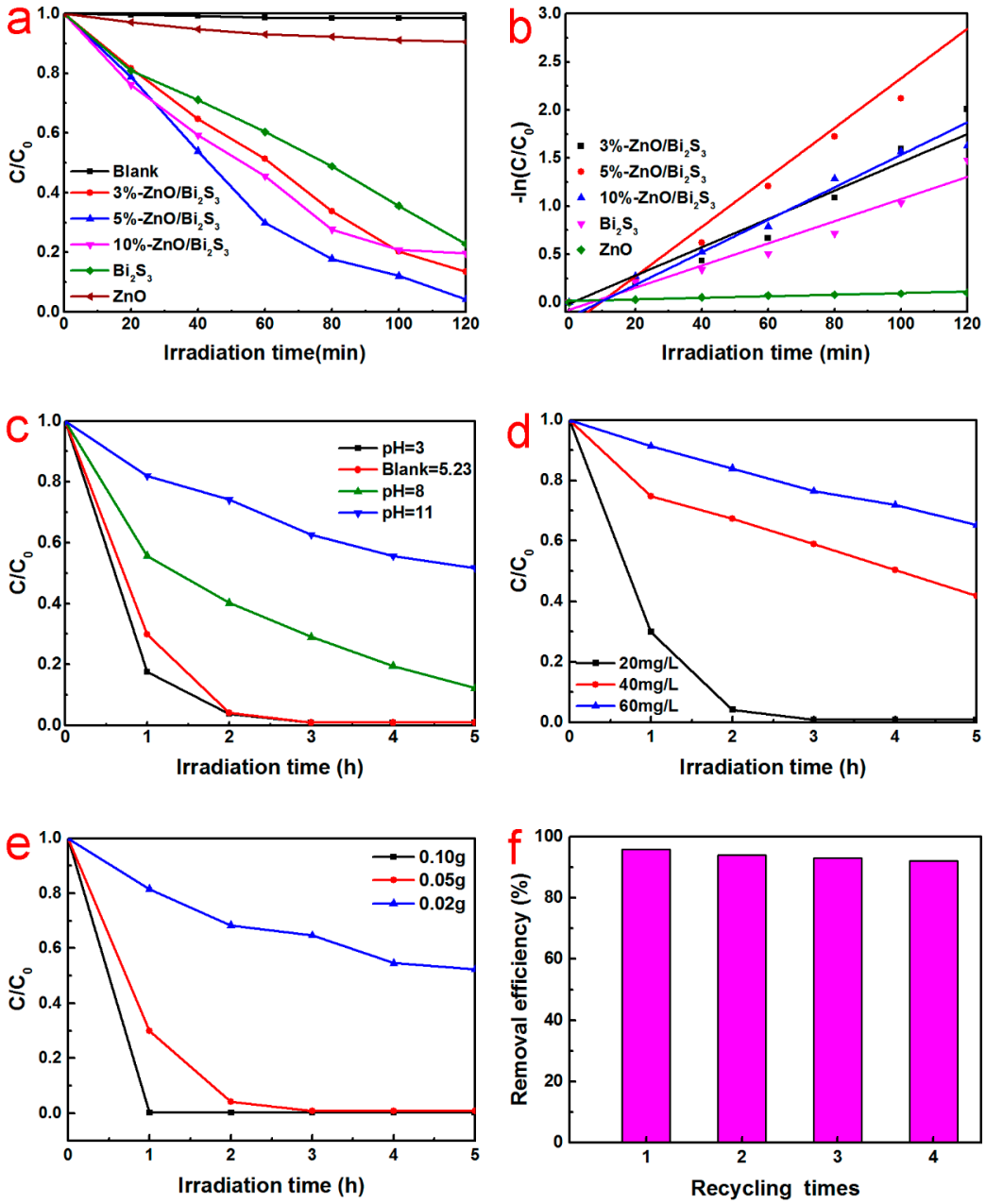

Figure 8. (**a**) Photocatalytic reduction of Cr(VI) (20 mg/L) under visible-light and (**b**) the corresponding pseudo-first-order kinetic curve using ZnO, Bi_2S_3 and ZnO/Bi_2S_3 composites; (**c**) effect of the initial solution pH; (**d**) initial Cr(VI) concentration; (**e**) catalyst dosage on the Cr(VI) photoreduction removal; and (**f**) cycling tests of photocatalytic activity of 5%-ZnO/Bi_2S_3 for the photoreduction of aqueous Cr(VI).

Figure 8c displays the effect of pH(adjusted by aqueous HCl or NaOH solution) on the removal efficiency of 5%-ZnO/Bi_2S_3 (20 mg/L aqueous Cr(VI)). When the initial solution pH was 3.0, 5%-ZnO/Bi_2S_3 removed 75.4% of aqueous Cr(VI) within 60 min. With the increasing of the solution pH (5.25, 8.0, and 11.0), the photoreduction efficiency of Cr(VI) decreased noticeably from 69.3%, 52.3% to 33.3%. On the one hand, the protonation of the catalyst surface will attract $HCrO_4^-$ and $Cr_2O_7^{2-}$ in acidic solution, which will promote the reduction of Cr (VI) [42]. On the other hand, when the solution is alkaline, the catalyst surface adsorbs a large amount of ·OH and the produced $Cr(OH)_3$ precipitates on its surface, which reduces the light harvesting, thus lowering the reduction removal of chromium ions [36].

Figure 8d depicts the effect of different initial Cr(VI) concentration for photoreduction removal using a 5%-ZnO/Bi_2S_3 photocatalyst. The degradation rate of Cr(VI) 20 mg/L was 95.9% within 2 h of visible light exposure. The degradation rates of Cr(VI) with incipient concentrations of 40 mg/L and 60 mg/L were 52% and 28% at the 6 h interval, respectively. A reason for this is the concentration of Chromium ion in the initial solution increases while the amount of catalyst feeding remains unchanged, which leads to more Cr(VI) ions adsorbing onto the catalyst solid, causing the decrease of adsorption sites on the photocatalyst, and thus decreasing the photoreduction efficiency of 5%-ZnO/Bi_2S_3 photocatalyst [43].

Figure 8e presents the effect of catalyst dosage for photocatalytic Cr(VI) reduction activity of 5%-ZnO/Bi_2S_3 composite. When 0.10 g of 5%-ZnO/Bi_2S_3 was used, the 100% Cr(VI) photoreduction removal was observed within 1 h's irradiation. With the decrease of the photocatalyst dosage to 0.02 g, the Cr(VI) reduction rate was dramatically reduced to only 42% in 5 h. This behavior could be attributed to a decrease in adsorption sites on the photocatalyst and a subsequent drop of photo-induced free electrons in the conduction band during photocatalysis.

To assess the stability and reusability of 5%-ZnO/Bi_2S_3 composite in the circulating tests for the photocatalytic reduction of Cr(VI) under visible-light irradiation, the photocatalyst solid was collected by centrifugation and washed with DI water prior to the addition of fresh Cr(VI) solution for the next run. From Figure 8f, 5%-ZnO/Bi_2S_3 photocatalyst exhibited no obvious change of the photocatalytic activity after four cycles with the removal rate still reaching 92%, suggesting that no significant damage of the structure of the composites took place and the as-prepared composite photocatalyst had excellent photo-stability and long-term reusability. Compared with bare ZnO with photocorrosion effect [44], the prepared photocatalyst had great potential for water remediation

2.3. Mechanism for Photocatalytic Cr(VI) Reduction

To make clear the possible reactive species involved in the ZnO/Bi_2S_3 catalyzed reduction of aqueous Cr(VI) under visible light irradiation, the species trapping experiments were conducted, in which BQ, IPA and CA were added as scavengers of·O_2^-,·OH and h^+ into Cr(VI) solution prior to the addition of the catalyst, respectively, and their final concentrations in the system were 0.1, 2.0, and 20.0 mmol/L, respectively. The trapping results are presented in Figure 9.

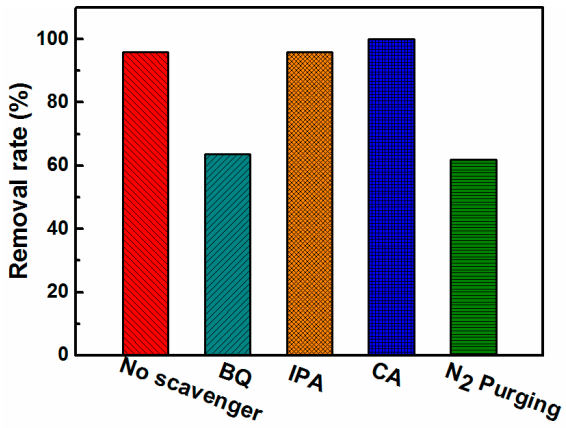

Figure 9. The effect of different reactive species scavengers on the Cr(VI) photo-degradation over 5%-ZnO/Bi_2S_3 composite.

The photocatalytic reduction of Cr(VI) was not affected in the presence of IPA, indicating that ·OH was not an active species in this photocatalytic system. The degradation rate of Cr(VI) was significantly reduced after the addition of BQ with only 60% removal rate in 2 h. The reason why BQ reduced the photocatalytic rate of Cr(VI) was that BQ captured electron-generated O_2^-, which reduced the amount of H_2O_2 according to the classical photo-catalysis mechanism, thereby decreasing the photoreduction removal rate of Cr(VI). Therefore,·O_2^- was the main active species in this photocatalytic reaction

process. Meanwhile, purging nitrogen gases dramatically reduced the photocatalytic rate of Cr(VI) from 95% to 56%. When O_2 was replaced by N_2, the reaction of successive species formation could not proceed and this phenomena was in good agreement with that of BQ scavenger, further suggesting that O_2^- played an important role in our photoreduction process. Upon the addition of CA, the photocatalytic activity of the 5%-ZnO/Bi_2S_3 composite toward Cr(VI) photoreduction was boosted and Cr(VI) was completely removed after 1 h of illumination. The consumption of h^+ by CA-trapping decreased the recombination of hole-electron pairs so that there were more electrons to participate in the photoreduction reaction. In brief, photo-excited e^- played a decisive role in our phtotoreduction of Cr(VI). Under air conditions, the intermediate H_2O_2 also contributed to the ZnO/Bi_2S_3-catalyzed reduction of acidic aqueous Cr(VI) under visible light irradiation.

Based on the above experimental results, a rational mechanism of ZnO/Bi_2S_3 photocatalyst for the improved photoreduction of Cr(VI) was raised (Figure 10). Bi_2S_3 could directly absorb the light of 400–700 nm to generate electrons (e^-) and holes (h^+), and electrons were excited from the valence band (VB) to CB, whereas ZnO (E_g = 3.2 eV) cannot be excited under visible light irradiation because of its broad energy gap. Because the CB (−0.33 eV) position of Bi_2S_3 [18] is more negative than that of ZnO [35] (−0.31 eV), the electrons of CB in Bi_2S_3 are rapidly transferred to ZnO and leave holes on the Bi_2S_3 VB. This is feasible in the laws of thermodynamics and the transfer is preferable due to the heterojunction of ZnO/Bi_2S_3 composites. Therefore, the photoinduced electrons and holes are separated efficiently. In the case of ZnO, its CB is more negative than E^θ ($Cr_2O_7^{2-}/Cr^{3+}$) = +1.33 eV (vs. NHE). The photo-induced electrons are accumulated to reduce Cr^{6+} to Cr^{3+} (Equation (2)). Meanwhile, due to the more positive VB (1.27 eV) position of Bi_2S_3 than the oxidation potential of E^θ (H_2O/O_2) = 1.23 eV (vs. NHE), the holes left on the VB of Bi_2S_3 oxidize H_2O to O_2 (Equation (3)). In addition, a portion of electrons located on the surface of the ZnO react with the adsorbed oxygen to produce $\cdot O_2^-$, which ultimately produces hydrogen peroxide (H_2O_2) (Equations (4) and (5)). Cr^{6+} is reduced to Cr^{3+} in acidic solution due to the strong reducibility of H_2O_2 [45]. The overall reaction process is illustrated by the following equations:

$$Cr_2O_7^{2-} + 14H^+ + 6e \rightarrow 2Cr^{3+} + 7H_2O \quad (2)$$

$$2H_2O + 4h^+ \rightarrow O_2 + 4H^+ \quad (3)$$

$$e + O_2 \rightarrow \cdot O_2^- \quad (4)$$

$$O_2^- + H^+ + H_2O \rightarrow H_2O_2 + \cdot OH \quad (5)$$

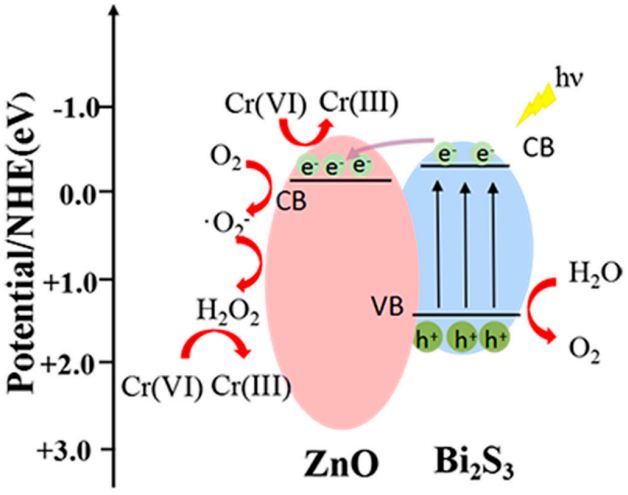

Figure 10. Schematic mechanism illustration of photoinduced electron-hole separation and transfer within ZnO/Bi_2S_3 composites for visible light-driven photoreduction of aqueous Cr(VI).

3. Experimental Section

3.1. Preparation of the Photocatalysts

All chemicals were of analytical grade purity in the experiments and without further purification. $Zn(CH_3COO)_2{\cdot}2H_2O$ (1.98 g) was dissolved in 50 mL of deionized (DI) water and vigorously stirred at 60 °C for 30 min. Forty milliliters of NaOH (0.3 mol/L) solution was added dropwise to adjust the solution to pH = 8. The mixture was further stirred for 60 min and then transferred into a 100 mL Teflon-lined autoclave and maintained at 160 °C for 12 h. After being cooled naturally to room temperature, the precipitate was filtered, washed successively with DI water and ethanol, and finally dried at 60 °C for 12 h. Pure ZnO powder was obtained by calcining this solid at 400 °C for 3 h.

Zero point zero six grams (0.06 g) of ZnO and 1.2 g of $Bi(NO_3)_3{\cdot}5H_2O$ were dissolved in ethylene glycol under the aid of sonication, and then 0.71 g of thioacetamide (TAA) was added to the solution and stirred for another 30 min. The mixture solution was poured into a 100 mL Teflon-lined stainless-steel autoclave and maintained at 160 °C for 18 h. The solids were centrifuged and washed with DI water and ethanol several times and dried at 80 °C for 5 h in air to obtain ZnO/Bi_2S_3 composite photocatalysts. By changing the amount of ZnO used in the procedure, three ZnO/Bi_2S_3 composites with 3%, 5% and 10% mass ratios of ZnO to Bi_2S_3 were synthesized, which were named as 3%-ZnO/Bi_2S_3, 5%-ZnO/Bi_2S_3 and 10%-ZnO/Bi_2S_3, respectively. For comparison, pure Bi_2S_3 was prepared with the same procedure without the use of ZnO.

3.2. Characterization

XRD was performed on a PANalytical X'pert Pro powder diffractometer (PANalytical, Almelo, The Netherlands) using Cu-Ka radiation (λ = 1.5418 Å) with a scan step of 0.013°. SEM images were generated with a Hitachi SU8020 (Hitachi Ltd., Tokyo, Japan) scanning electron microscope with an acceleration voltage of 20KV. HRTEM was performed on a FEI Tecnai G2 F20 field-emission transmission electron microscopy (FEI Inc.,, Hillsboro, OR, USA) at an acceleration voltage of 200 KV. XPS measurements were performed on a Thermo Fisher ESCALAB 250Xi photoelectron spectrometer (Thermo Fisher Scientific Inc., Waltham, MA, USA) using a monochromatic Al KαX-ray source (hν = 1486.6 eV). DRS spectrum was recorded on a Hitachi U-4100 UV-vis spectrophotometer (Hitachi, Tokyo, Japan) using $BaSO_4$ as the reference sample. Photoelectrochemical measurements were conducted in a three electrodes quartz cell with 0.1 M Na_2SO_4 solution on the electrochemical system (CHI-760E, Shanghai Chenhua Instruments, Shanghai, China). PL spectra were recorded in a Hitachi F-7000 fluorescence spectrophotometer (Hitachi, Tokyo, Japan).

3.3. Photocatalytic Tests

The photocatalytic Cr(VI) reduction performance of ZnO/Bi_2S_3 samples under visible light was conducted by a 500 W Xe lamp (BILON-CHX-V, Shanghai photoreactor, BiLon, Shanghai, China) with maximum wavelength emission at 470 nm. The lamp was placed in a trap with running water circulating through a jacket in order to maintain a constant temperature in the reaction system, and the distance between the light source and the tube containing the reaction mixture was set to be 15 cm. Stock solution (100 mg/L) of Cr(VI) was prepared by dissolving $K_2Cr_2O_7$(analytical grade, Kelong Reagent Factory, Chengdu, China) into distilled water. In a typical procedure, 0.05 g of the photocatalyst was added to 50 mL of Cr(VI) solution (20 mg/L), and the suspension was stirred in the dark for 60 min to reach the adsorption–desorption equilibrium. Then, the solution was exposed to light irradiation under magnetic stirring. During the irradiation, 4 mL of the reaction solution was withdrawn at certain time intervals and centrifuged to remove the photocatalyst from the solution. The Cr(VI) concentration in the supernatant solution was determined spectrophotometrically at 540 nm using the diphenylcarbazide method [46] by UV-1000 spectrophotometer (AOE, Shanghai, China).

The initial solution pH was adjusted by 0.01 mg/L aqueous HCl or 0.01 mg/L NaOH solutions. For comparison, the blank experiments to test the Cr(VI) stability under irradiation without any

photocatalysts and the dark experiments to test the physical adsorption capacity of the photocatalysts were conducted with no irradiation under the identical conditions. For the radical species trapping tests, Benzoquinone (BQ), Iso-propyl alcohol (IPA) and Citric Acid (CA) were introduced into Cr(VI) solution prior to the addition of the catalyst as the scavengers of $\cdot O_2^-$,·OH and h^+, respectively [47].

4. Conclusions

Briefly, ZnO/Bi_2S_3 nanocomposites were prepared via a facile solvothermal method. Detailed characterization showed the introduction of ZnO played a key role in the formation of the heterojunction structure of sandwiched-like ZnO/Bi_2S_3, where some tiny ZnO nanoparticles were randomly embedded between Bi_2S_3 nanoflakes. The enhanced photocatalytic reduction activity towards aqueous Cr(VI) revealed that there was a synergistic effect between the two components of the composites. The mechanism strongly suggested that the enhanced visible-light-driven photoreduction performance of ZnO/Bi_2S_3 photocatalyst was ascribed to the increased light harvesting and the effective separation and transfer of the photogenerated charge carriers across the heterojunction interface of the ZnO/Bi_2S_3 composite. The photocatalysts prepared herein in the study were evaluated by photodegrading other wastewater pollutants and had great potential in environmental remediation.

Supplementary Materials: The following are available online at http://www.mdpi.com/2073-4344/9/7/624/s1, Figure S1: Figure S1. SEM image of Bi_2S_3 (a), the element composition (b) and elementary mapping of Bi (c) and S (d). Figure S2: Figure S2. SEM image of 5%-ZnO/Bi_2S_3 (a), the element composition (b) and elementary mapping of Bi (c), S (d), Zn (e) and O (f).

Author Contributions: Investigation, X.W.; Methodology, Z.F., W.J. and C.L.; Project administration, X.Y.; Supervision, X.Y. and X.Z.; Writing—original draft, X.W.; Writing—review & editing, X.Y.

Funding: This research was funded by the National Natural Science Foundation of China, grant number 51402030. Science and Technology Research Program of Chongqing Municipal Education Commission, grant number KJZD-K201800703. The APC was funded by Natural Science Foundation of the Chongqing Science and Technology Commission, grant number cstc2017jcyjBX0028.

Conflicts of Interest: The authors declare no conflict of interest.

References

1. Fan, Q.; Wang, R.; Li, G.; Fan, T.; Zhao, H.; Rong, C. Highly efficient photocatalytic reduction of Cr(VI) by bismuth hollow nanospheres. *Catal. Commun.* **2013**, *42*, 14–19.
2. Fırlak, M.; Kahrman, M.V.; Yetimoğlu, E.K. Removal of Ag(I) from Aqueous Solutions by Thiol-ene-Based Hydrogel and Its Application to Radiographic Films. *Water Air Soil Pollut.* **2014**, *225*, 1843. [CrossRef]
3. Daneshvar, N.; Salari, D.; Aber, S. Chromium adsorption and Cr(VI) reduction to trivalent chromium in aqueous solutions by soya cake. *J. Hazard. Mater.* **2002**, *94*, 49–61. [CrossRef]
4. Maheshwari, U.; Gupta, S. Removal of Cr(VI) from wastewater using activated neem bark in a fixed-bed column: Interference of other ions and kinetic modelling studies. *Desalin. Water Treat.* **2016**, *57*, 8514–8525. [CrossRef]
5. Patel, H.A.; Karadas, F.; Byun, J.; Park, J.; Yavuz, C.T. Highly stable nanoporous sulfur-bridged covalent organic polymers for carbon dioxide removal. *Adv. Funct. Mater.* **2013**, *23*, 2270–2276. [CrossRef]
6. Wang, L.; Zeng, T.; Liao, G.; Cheng, Q.; Pan, Z. Syntheses, structures and catalytic mechanisms of three new MOFs for aqueous Cr(VI) reduction and dye degradation under UV light. *Polyhedron* **2018**, *157*, 152–162. [CrossRef]
7. Marinho, B.A.; Cristóvão, R.O.; Djellabi, R.; Loureiro, J.M.; Rui, A.R.B.; Vilar, V.J.P. Photocatalytic reduction of Cr(VI) over TiO_2-coated cellulose acetate monolithic structures using solar light. *Appl. Catal. B Environ.* **2017**, *203*, 18–30. [CrossRef]
8. Megan, G.; Yu, P.C.; Hug, S.J.; Barbara, S. Role of dissolved organic matter composition on the photoreduction of Cr(VI) to Cr(III) in the presence of iron. Environ. *Sci. Technol.* **2003**, *37*, 4403–4409.
9. Wang, X.; Pehkonen, S.O.; Ray, A.K. Removal of Aqueous Cr(VI) by a Combination of Photocatalytic Reduction and Coprecipitation. *Ind. Eng. Chem. Res.* **2004**, *43*, 1665–1672. [CrossRef]

10. Chanchal, M.; Mainak, G.; Jaya, P.; Anindita, R.; Jayasmita, J.; Tarasankar, P. Morphology controlled synthesis of SnS_2 nanomaterial for promoting photocatalytic reduction of aqueous Cr(VI) under visible light. *Langmuir* **2014**, *30*, 4157–4164.
11. Wang, L.; Nan, W.; Zhu, L.; Yu, H.; Tang, H. Photocatalytic reduction of Cr(VI) over different TiO_2 photocatalysts and the effects of dissolved organic species. *J. Hazard. Mater.* **2008**, *152*, 93–99. [CrossRef]
12. Rengaraj, S.; Venkataraj, S.; Yeon, J.W.; Kim, Y.; Li, X.Z.; Pang, G.K.H. Preparation, characterization and application of Nd–TiO_2 photocatalyst for the reduction of Cr(VI) under UV light illumination. *Appl. Catal. B Environ.* **2007**, *77*, 157–165. [CrossRef]
13. Ge, Z.H.; Zhang, B.P.; Yu, Z.X.; Jiang, B.B. Controllable synthesis: Bi_2S_3 nanostructure powders and highly textured polycrystals. *Crystengcomm* **2012**, *14*, 2283–2288. [CrossRef]
14. Liu, Z.; Peng, S.; Xie, Q.; Hu, Z.; Yang, Y.; Zhang, S.; Qian, Y. Large-Scale Synthesis of Ultralong Bi_2S_3 Nanoribbons via a Solvothermal Process. *Adv. Mater.* **2010**, *15*, 936–940. [CrossRef]
15. Sarkar, A.; Ghosh, A.B.; Saha, N.; Srivastava, D.N.; Paul, P.; Adhikary, B. Enhanced photocatalytic performance of morphologically tuned Bi_2S_3 NPs in the degradation of organic pollutants under visible light irradiation. *J. Colloid Interface Sci.* **2016**, *483*, 9–59. [CrossRef]
16. Hu, E.; Gao, X.; Etogo, A.; Xie, Y.; Zhong, Y.; Yong, H. Controllable one-pot synthesis of various one-dimensional Bi_2S_3 nanostructures and their enhanced visible-light-driven photocatalytic reduction of Cr(VI). *J. Alloy. Compd.* **2014**, *611*, 335–340. [CrossRef]
17. Ding, Y.H.; Zhang, X.L.; Zhang, N.; Zhang, J.Y.; Zhang, R.; Liu, Y.F.; Fang, Y.Z. A visible-light driven Bi_2S_3@ZIF-8 core-shell heterostructure and synergistic photocatalysis mechanism. *Dalton Trans.* **2017**, *47*, 684–692. [CrossRef]
18. Sun, H.; Jiang, Z.; Wu, D.; Ye, L.; Wang, T.; Wang, B.; An, T.; Wong, P.K. Defect-type-dependent near-infrared-driven photocatalytic bacterial inactivation by defective Bi_2S_3 nanorods. *Chemsuschem* **2019**, *12*, 890–897. [CrossRef]
19. Chen, Y.; Tian, G.; Guo, Q.; Rong, L.; Fu, H. One-step synthesis of Hierarchical Bi_2S_3 nanoflower\In_2S_3 nanosheet composite with efficient visible light photocatalytic activity. *Crystengcomm* **2015**, *17*, 8720–8727. [CrossRef]
20. Vattikuti, S.V.P.; Shim, J.; Chan, B. 1D Bi_2S_3 nanorod/2D e-WS_2 nanosheet heterojunction photocatalyst for enhanced photocatalytic activity. *J. Solid State Chem.* **2018**, *258*, 526–535. [CrossRef]
21. Chen, Y.; Tian, G.; Mao, G.; Rong, L.; Xiao, Y.; Han, T. Facile synthesis of well-dispersed Bi_2S_3 nanoparticles on reduced graphene oxide and enhanced photocatalytic activity. *Appl. Surf. Sci.* **2016**, *378*, 231–238. [CrossRef]
22. Ge, Z.H.; Qin, P.; He, D.; Chong, X.; Feng, D.; Ji, Y.H.; Feng, J.; He, J. Highly enhanced thermoelectric properties of Bi/Bi_2S_3 nano composites. *ACS Appl. Mater. Interfaces* **2017**, *9*, 4828–4834. [CrossRef]
23. Wang, Y.; Jin, J.; Chu, W.; Cahen, D.; He, T. Synergistic effect of charge generation and separation in epitaxially grown BiOCl/Bi_2S_3 nano-heterostructure. *ACS Appl. Mater. Interfaces* **2018**, *10*, 15304–15313. [CrossRef]
24. Yang, L.; Sun, W.; Luo, S.; Yan, L. White fungus-like mesoporous Bi_2S_3 ball/TiO_2 heterojunction with high photocatalytic efficiency in purifying 2,4-dichlorophenoxyacetic acid/Cr(VI) contaminated water. *Appl. Catal. B Environ.* **2014**, *156*, 25–34. [CrossRef]
25. Rauf, A.; Sher Shah, M.S.A.; Choi, G.H.; Humayoun, U.B.; Yoon, D.H.; Bae, J.W.; Park, J.; Kim, W.J.; Yoo, P.J. Facile synthesis of hierarchically structured Bi_2S_3/Bi_2WO_6 photocatalysts for highly efficient reduction of Cr(VI). *ACS Sustain. Chem. Eng.* **2015**, *3*, 2847–2855. [CrossRef]
26. Jing, C.; Benyan, X.; Haili, L.; Bangde, L.; Shifu, C. Novel heterostructured Bi_2S_3/BiOI photocatalyst: Facile preparation, characterization and visible light photocatalytic performance. *Dalton Trans.* **2012**, *41*, 11482–11490.
27. Senthilvelan, S.; Chandraboss, V.L.; Kamalakkannan, J.; Prabha, S. An Efficient Removal of Methyl Violet from Aqueous Solution by AC-Bi/ZnO Nanocomposite Material. *RSC Adv.* **2015**, *5*, 25857–25869.
28. Yang, L.; Xu, C.; Wan, F.; He, H.; Gu, H.; Xiong, J. Synthesis of RGO/BiOI/ZnO composites with efficient photocatalytic reduction of aqueous Cr(VI) under visible-light irradiation. *Mater. Res. Bull.* **2019**, *112*, 154–158. [CrossRef]
29. Subramanian, B.; Meenakshisundaram, S. The simple, template free synthesis of a Bi_2S_3-ZnO heterostructure and its superior photocatalytic activity under UV-A light. *Dalton Trans.* **2013**, *42*, 5338–5347.
30. Zheng, L.; Deng, J.; Wang, L.; Wang, L.; Teng, F.; Tong, Z. Toluene and ethanol sensing performances of pristine and PdO-decorated flower-like ZnO structures. *Sens. Actuators B* **2013**, *176*, 323–329.

31. Shu, F.W.; Feng, G.; Zhong, S.Y.; Meng, K.L.; Zhou, G.J.; Wen, G.Z. Facile synthesis of silica-coated Bi_2S_3 nanorods and hollow silica nanotubes. *J. Cryst. Growth* **2015**, *282*, 79–84.
32. Hang, X.; Zhang, J.; Yu, J.Q.; Zhang, Y.; Cui, Z.X.; Sun, Y.; Hou, B. Fabrication of InVO4/AgVO3 heterojunctions with enhanced photocatalytic antifouling efficiency under visible-light. *Appl. Catal. B Environ.* **2018**, *220*, 57–66.
33. Yu, J.; Jiang, C.; Guan, Q.; Ning, P.; Gu, J.; Chen, Q.; Zhang, J.; Miao, R. Enhanced removal of Cr(VI) from aqueous solution by supported ZnO nanoparticles on biochar derived from waste water hyacinth. *Chemosphere* **2017**, *195*, 632–640. [CrossRef]
34. Wang, M.; Yang, L.; Yuan, J.; He, L.; Song, Y.; Zhang, H.; Zhang, Z.; Fang, S. Heterostructured Bi_2S_3@NH_2-MIL-125(Ti) nanocomposite as a bifunctional photocatalyst for Cr(VI) reduction and rhodamine B degradation under visible light. *RSC Adv.* **2018**, *8*, 12459–12470. [CrossRef]
35. Yuan, X.; Jing, Q.; Chen, J.; Li, L. Photocatalytic Cr(VI) reduction by mixed metal oxide derived from ZnAl layered double hydroxide. *Appl. Clay Sci.* **2017**, *143*, 168–174. [CrossRef]
36. Yuan, X.Y.; Cheng, X.; Jing, Q.Y.; Niu, J.W.; Peng, D.; Feng, Z.J.; Wu, X. ZnO/$ZnAl_2O_4$ Nanocomposite with 3D Sphere-Like Hierarchical Structure for Photocatalytic Reduction of Aqueous Cr(VI). *Materials* **2018**, *11*, 1624. [CrossRef]
37. Wang, X.; Rong, L.; Kang, W. Synthesis of ZnO@ZnS–Bi_2S_3 core–shell nanorod grown on reduced graphene oxide sheets and its enhanced photocatalytic performance. *J. Med. Chem. A* **2014**, *2*, 8304–8313.
38. Duan, Y.; Stinespring, C.D.; Chorpening, B. Electronic Structures, Bonding Configurations, and Band-Gap-Opening Properties of Graphene Binding with Low-Concentration Fluorine. *Chemistryopen* **2015**, *4*, 642–650. [CrossRef]
39. Xu, T.; Zhang, L.; Cheng, H.; Zhu, Y. Significantly enhanced photocatalytic performance of ZnO via graphene hybridization and the mechanism study. *Appl. Catal. B Environ.* **2011**, *101*, 382–387. [CrossRef]
40. Kumar, S.; Sharma, S.; Umar, A.; Kansal, S.K. Bismuth Sulphide (Bi_2S_3) Nanotubes as an Efficient Photocatalyst for Methylene Blue Dye Degradation. *Nanosci. Nanotechnol. Lett.* **2016**, *8*, 266–272. [CrossRef]
41. Chalermchai, P.; Somchai, T.; Titipun, T. Environmentally benign synthesis of Bi_2S_3 quantum dot using microwave-assisted approach. *J. Nanosci. Nanotechnol.* **2013**, *13*, 2189–2192.
42. Nan, W.; Zhu, L.; Deng, K.; She, Y.; Yanmin, Y.U.; Tang, H. Visible light photocatalytic reduction of Cr(VI) on TiO_2 in situ modified with small molecular weight organic acids. *Appl. Catal.* **2010**, *95*, 400–407.
43. Barrera, C.E. A review of chemical, electrochemical and biological methods for aqueous Cr(VI) reduction. *J. Hazard. Mater.* **2012**, *223*, 1–12. [CrossRef]
44. Yuan, X.Y.; Feng, Z.; Zhao, J.; Niu, J.; Liu, J.; Peng, D.; Cheng, X. Significantly enhanced aqueous Cr(VI) removal performance of Bi/ZnO nanocomposites via synergistic effect of adsorption and SPR-promoted visible light photoreduction. *Catalysts* **2018**, *8*, 426. [CrossRef]
45. Bhati, A.; Anand, S.R.; Saini, D.; Sonkar, S.K. Sunlight-induced photoreduction of Cr(VI) to Cr(III) in wastewater by nitrogen-phosphorus-doped carbon dots. *NPJ Clean Water* **2019**, *2*, 12. [CrossRef]
46. Yuan, X.; Chao, Z.; Jing, Q.; Qi, T.; Mu, Y.; Du, A. Facile Synthesis of g-C_3N_4Nanosheets/ZnO Nanocomposites with Enhanced Photocatalytic Activity in Reduction of Aqueous Chromium(VI) under Visible Light. *Nanomaterials* **2016**, *6*, 173. [CrossRef]
47. Li, B.; Lai, C.; Zeng, G.; Qin, L.; Yi, H.; Huang, D.; Zhou, C.; Liu, X.; Cheng, M.; Xu, P. Facile hydrothermal synthesis of Z-scheme $Bi_2Fe_4O_9$/Bi_2WO_6 heterojunction photocatalyst with enhanced visible light photocatalytic activity. *ACS Appl. Mater. Interfaces* **2018**, *10*, 18824–18836. [CrossRef]